A General Strategy to Superstructured Networks and Nested Self-Similar Networks of Bismuth Compounds

Chuan Fei Guo, Jianming Zhang, Ye Tian, and Qian Liu*

National Center for Nanoscience and Technology, China, No. 11 Beiyitiao, Zhongguancun, Beijing 100190, China

ABSTRACT

We have reported the synthesis of superstructured nanonetworks of BiOCl and nested nanonetworks of Bi_2S_3 in a series of lattice-directed topotactic transformations [C. F. Guo *et al. J. Am. Chem. Soc.* 2011, *138*, 8211−8215]. Here we extend the transformations to a much broader system including ordered nanowall networks of BiOCl, BiOBr, $Bi_2O_2CO_3$, β-Bi_2O_3, and Bi_2S_3, as well as nested self-similar networks of Bi_2S_3 and amorphous BiO_x. We suggest even more superstructured networks and nested self-similar networks of bismuth compounds with a lattice parameter of $\sim 2^{n/2} \times 3.9$ Å (n = 0, 1, 2, 3, 4), might also be obtained. The superstructured networks and nested networks are novel architectures that may find applications in electronic devices, sensors, filters, and photocatalysts.

KEYWORDS: bismuth compounds · superstructure · network · lattice match · toptactic transformation

Designing and synthesizing nanostructured materials, especially those ordered and superstructured semiconductors with facet dominated growth and properties are significant for high performance devices and systems. Single crystalline building blocks or hierarchical structures composed of single crystalline building blocks are often ideal units for this purpose. In the past decade, a great amount of facet dominated single crystal building blocks, for example, nanowires,[1−3] nanorods,[4,5] nanobelts,[6,7] nanoplates,[7] and nanorings[8] have been synthesized. Ordered arrays and hierarchical nanostructures made up of single crystalline building blocks have also been obtained.[9−11] Sequential growth of different nanostructures, such as ZnO/SnO_2, Co_3O_4@MnO_2, and Fe_3O_4/$CoSe_2$ nanostructures could lead to novel architectures and enhanced properties.[12−14] As one of the challenges, it is still difficult to synthesize ordered architectures made up of two-dimensional (2D) building blocks, which might be useful in supercapacitors, energy storage, and gas sensing. In our previous work, we successfully synthesized 2D orthogonal networks (2DONWs) of BiOCl nanowall, and nested self-similar 2D orthogonal networks (N2DONWs) of Bi_2S_3 nanorods.[15] We believe the novel architectures could be extended to many other bismuth compounds according to their similarity in crystal structure.

Many bismuth compounds have a crystal structure with a 4-fold symmetry (*e.g.*, tetragonal or cubic β-Bi_2O_3, γ-Bi_2O_3, δ-Bi_2O_3, $Bi_2O_{2.33}$, $Bi_2O_2CO_3$, BiOX (X = Cl, Br), $BiFeO_3$, Bi_2O_2Se, and $C_2H_3BiO_3$) or quasi 4-fold symmetry (*e.g.*, orthorhombic Bi_2S_3, Bi_2WO_6, Bi_2MoO_6, and Bi_2VO_5) and a lattice parameter of $\sim 2^{n/2} \times 3.9$ Å (n = 0, 1, 2, 3, 4). And interestingly, many single crystalline nanostructures of such materials tend to present layered morphologies, because of weak nonbonding interaction (van der Waals force) among the *c*-planes, or strong polarization along the *c*-axis.[15−18] These characteristics make it possible to synthesize superstructured 2D nanostructures of bismuth compounds in a series of topotactic transformations.[15,19] The 2DONWs of BiOCl nanowall, and nested self-similar N2DONWs of Bi_2S_3 are a successful demonstration of sequential topotactic tranformations that lead to complex and/or hierarchical superstructures, by using 2D building blocks as the template.[15] However, we would like to alert that this route is only one out of many processes that can result in the formation of 2DONWs and N2DONWs of bismuth compounds. Here we show the synthesis of β-Bi_2O_3, $Bi_2O_2CO_3$, BiOCl, BiOBr, and Bi_2S_3 2DONWs, together with Bi_2S_3 and amorphous BiO_x self-similar N2DONWs, in mild conditions. And we predict that there shall be 2DONWs and N2DONWs of many other bismuth compounds (but not limited to), such as $Bi_2O_{2.33}$, $BiFeO_3$, Bi_2WO_6, Bi_2O_2Se, and Bi_2MoO_6 due to lattice match.

* Address correspondence to liuq@nanoctr.cn.

Received for review June 1, 2012 and accepted September 7, 2012.

Published online September 08, 2012
10.1021/nn303467r

RESULTS AND DISCUSSION

The bismuth compounds involved in this study are tetragonal (t) β-Bi_2O_3, BiOX (X = Cl, Br), $Bi_2O_2CO_3$, and orthorhombic (o) Bi_2S_3, whose lattice parameters are listed in Table 1. The {200} facets of β-Bi_2O_3, the {100} facets of BiOCl, BiOBr, and $Bi_2O_2CO_3$, as well as the (001) facet of Bi_2S_3, all have a *d*-spacing close to 3.90 Å. The design and fabrication of related superstructures are based on lattice match among these phases. Lattice misfit is defined as

$$f = \frac{|d - d_s|}{d_s} \quad (1)$$

where d is an interplanar spacing of the emerging phase, and d_s is the corresponding spacing of the substrate or precursor.

Synthesis and Characterization of BiOX (X = Cl, Br) 2DONWs and Bi_2S_3 N2DONWs. Tetragonal β-Bi_2O_3 (lattice parameters a = 7.741 Å and c = 5.634 Å) films obtained by annealing BiO_x films were used as the precursors for all nanostructures in the study. During crystallization of the amorphous films, many randomly oriented single crystalline domains with an average diameter of ~25 μm were formed. As presented in our previous work, the β-Bi_2O_3 domains could transform to BiOCl (lattice parameters a = 3.887 Å and c = 7.354 Å) 2DONWs in diluted hydrochloric acid (HCl), with an epitaxial relationship of $(110)_{BiOCl}||(220)_\beta$, $(110)_{BiOCl}||(220)_\beta$, and $[001]_{BiOCl}||[001]_\beta$ for one set of nanowalls and $(110)_{BiOCl\perp}||(002)_\beta$, $(110)_{BiOCl\perp}||(220)_\beta$, and $[001]_{BiOCl\perp}||[110]_\beta$ for the other set of nanowalls in the perpendicular direction (marked by `⊥'),[15] as shown in the scanning electron microscopy (SEM) image and schematic plan in Figure 1 panels a and b, respectively. A BiOCl nanowall could then transform to a Bi_2S_3 network of nanorods, with the presence of S^{2-} (Figure 1c). We used a blended solution of thioacetamide (TAA, 0.04 M) and HCl (0.02 M) to produce S^{2-}.

BiOBr also has a tetragonal structure, with lattice parameters a = 3.927 Å and c = 8.101 Å. The *d*-spacing of the $\{110\}_{BiOBr}$ facets is 2.78 Å, close to that of the $\{220\}_\beta$. Therefore, BiOBr could also form epitaxial 2DONWs of nanowalls (Figure 1d). However, the formed BiOBr 2DONWs do not present very good ordering, probably because of the larger lattice misfit. Similar to BiOCl, a BiOBr 2DONW can also transform to Bi_2S_3 N2DONW (Figure 1e), and corresponding solution is blended TAA (0.04 M), NaBr (0.02 M), and H_2SO_4 (0.01 M).

Synthesis and Characterization of $Bi_2O_2CO_3$ 2DONWs. A β-Bi_2O_3 film (which is transparent) incubated in blended solution of $NaHCO_3$ (0.04 M) and HNO_3 (0.02 M) at 60 °C for 5 h could convert to a white film. SEM images in Figure 2a,b show that the white film is made up of many 2DONWs of nanowalls, which are typically 5−10 nm in thickness and 300 nm in length. The morphology is very similar to the BiOCl 2DONWs.

TABLE 1. Lattice Parameters of the Materials in This Study

	lattice parameters (Å)				
materials	*a*	*b*	*c*	structure	lattice misfit[a]
β-Bi_2O_3	7.741	7.741	5.634	t	
BiOCl	3.887	3.887	7. 354	t	0.43% (d_{100})
BiOBr	3.927	3.927	8.101	t	1.5% (d_{100})
$Bi_2O_2CO_3$	3.865	3.865	13.67	t	0.14% (d_{100})
Bi_2S_3	11.14	11.30	3.981	o	2.9% (d_{001})

[a] Lattice misfit in reference to d_{200} (3.871 Å) of β-Bi_2O_3.

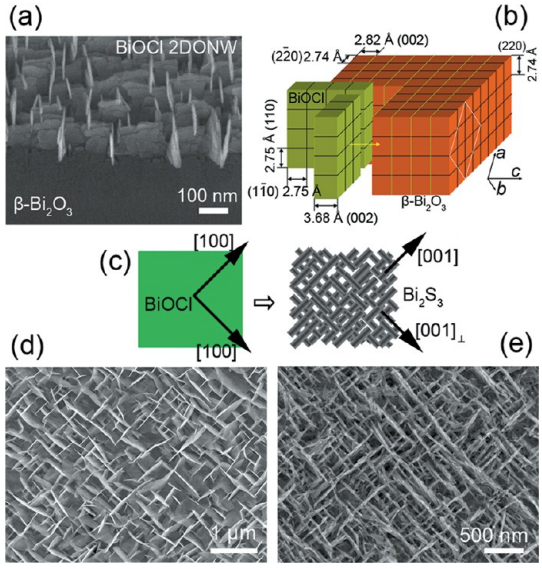

Figure 1. (a) Tilt view of a BiOCl 2DONW grown from β-Bi_2O_3. (b) Schematic illustration on the epitaxial relationship between BiOCl nanowalls and β-Bi_2O_3. (c) Epitaxial relationship between BiOCl nanowall and Bi_2S_3 network. (d) Epitaxial BiOBr 2DONW. (e) Bi_2S_3 N2DONW transformed from a BiOBr 2DONW.

Crystal structure of a single nanowall was investigated by using high-resolution transmission electron microscopy (HRTEM) and selected area electron diffraction (SAED). Figure 2c is a bright field TEM image of a nanowall, while Figure 2 panels d and e are corresponding SAED pattern and HRTEM image taken perpendicularly to the nanowall plane, showing a 4-fold symmetry with a *d*-spacing of 2.74 Å. Figure 2f is a HRTEM image taken from the side, for which the *d*-spacings of 6.80 Å and 2.74 Å belong to the {002} and {110} planes of tetragonal $Bi_2O_2CO_3$ (lattice parameters a = b = 3.865 Å, and c = 13.67 Å). We can see from Figure 2e that the thickness of the nanowall is about 5.5 nm, exactly 4 times the (001) *d*-spacing, implying the nanowall is made up of four monolayers stacking along the *c*-axis. Upon our observation, most of the nanowalls are made of only several monolayers. This strongly anisotropic growth should be ascribed to the weak nonbonding interaction in the *c*-planes.[15]

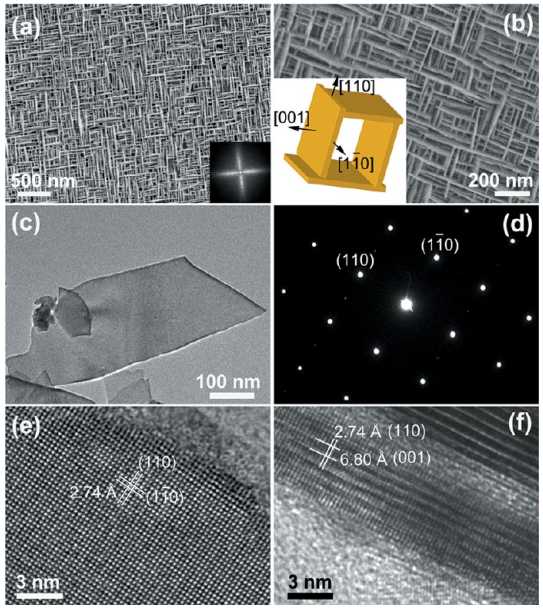

Figure 2. (a) SEM image of a $Bi_2O_2CO_3$ 2DONW, showing two sets of nanowalls aligned perpendicularly. Inset is the corresponding Fourier transformation pattern. (b) Magnified SEM image of a $Bi_2O_2CO_3$ 2DONW, inset indicates crystal orientations of the nanowall. (c) Bright field TEM image of a $Bi_2O_2CO_3$ nanowall. (d) SAED pattern corresponding to the nanowall in panel c shows a 4-fold symmetry. (e) HRTEM image taken along the [001] zone axis of the nanowall in panel c. (f) HRTEM of a $Bi_2O_2CO_3$ nanowall taken along the [1$\bar{1}$0] zone axis. The nanowall is about 5.5 nm in thickness.

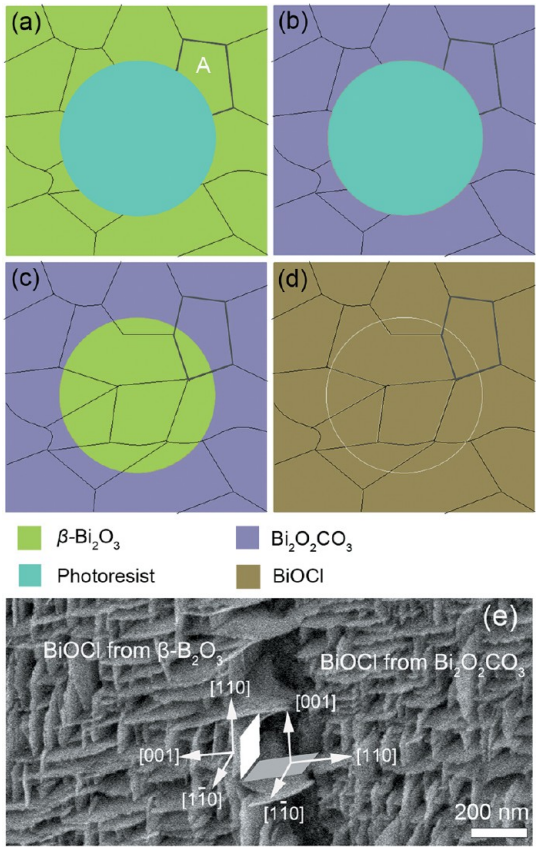

Figure 3. Determination of the epitaxial relationship between $Bi_2O_2CO_3$ and β-Bi_2O_3. (a) A drop of photoresist on a β-Bi_2O_3 film, shading some crystalline domains. (b) Nonshaded β-Bi_2O_3 converts to $Bi_2O_2CO_3$. (c) Removal of the photoresist. (d) Both $Bi_2O_2CO_3$ 2DONWs and β-Bi_2O_3 domains convert to BiOCl 2DONWs. (e) SEM image of two BiOCl 2DONWs from β-Bi_2O_3 and $Bi_2O_2CO_3$ 2DONW, respectively. The left half was once shaded by photoresist.

The $Bi_2O_2CO_3$ 2DONWs can also be formed in other solution which can generate CO_2, *e.g.*, blended solution of Na_2CO_3 and HNO_3, and blended solution of $NaHCO_3$ and CH_3COOH. Concentrations of the reagents should be low to avoid CO_2 bubbles. An acidic environment is also important for the formation of the unique nanostructures because β-Bi_2O_3 needs to be etched before a new phase emerges.

Structural Relations between $Bi_2O_2CO_3$ and β-Bi_2O_3. Exploring structural relationship among the $Bi_2O_2CO_3$ nanowall and β-Bi_2O_3 is significant and interesting. In our previous work, we used focused ion beam (FIB) milling to make TEM specimen to investigate the epitaxial relationship between BiOCl 2DONW and β-Bi_2O_3 film.[15] FIB milling is unquestionably an effective and visualized technique to fabricate TEM specimen and thus to understand crystal structure information. However, fabricating TEM specimen by FIB milling is rather costly and time-consuming. We tactfully avoid the use of FIB, while show intuitively the structural relationship of $Bi_2O_2CO_3$ and β-Bi_2O_3 in an SEM observation. BiOCl 2DONW is introduced here as a reference object since its structural relationship with β-Bi_2O_3 has already been known.

A small drop of photoresist (MircoChem SU-8) on a β-Bi_2O_3 film can partially shade some β-Bi_2O_3 domains (exemplified by the domain marked with `A'), as schematically shown in Figure 3a. Then the sample is incubated in a preblended solution of $NaHCO_3$ (0.04 M) and HNO_3 (0.02 M) for 5 h, leading to the formation of $Bi_2O_2CO_3$ 2DONWs in the nonshaded β-Bi_2O_3 (Figure 3b) film. After that, the photoresist is removed in acetone and β-Bi_2O_3 becomes exposed (Figure 3c). Finally, the sample is dipped in diluted HCl solution (0.10 M) for 30 s, during which both single crystalline β-Bi_2O_3 and $Bi_2O_2CO_3$ 2DONWs transform to BiOCl 2DONWs (Figure 3d). Figure 3e shows a SEM image of a domain (that used to be partially covered by photoresist, like the domain `A') made of two parts: a BiOCl 2DONW from $Bi_2O_2CO_3$ 2DONW (a $Bi_2O_2CO_3$ nanowall could transform to a BiOCl nanowall without changing morphology, which will be discussed in the next part), and a BiOCl 2DONW from β-Bi_2O_3. The two parts have a similar morphology and exactly the same crystalline orientations, implying that $Bi_2O_2CO_3$ and BiOCl have a similar epitaxial relation with β-Bi_2O_3. That is, $(110)_{Bi_2O_2CO_3}\|(220)_\beta$, $(1\bar{1}0)_{Bi_2O_2CO_3}\|(2\bar{2}0)_\beta$, and $[001]_{Bi_2O_2CO_3}\|[001]_\beta$; $(110)_{Bi_2O_2CO_3\perp}\|(002)_\beta$, $(1\bar{1}0)_{Bi_2O_2CO_3\perp}\|(2\bar{2}0)_\beta$, and $[001]_{Bi_2O_2CO_3\perp}\|[110]_\beta$. The epitaxial growth of $Bi_2O_2CO_3$ from β-Bi_2O_3 is related to their good lattice

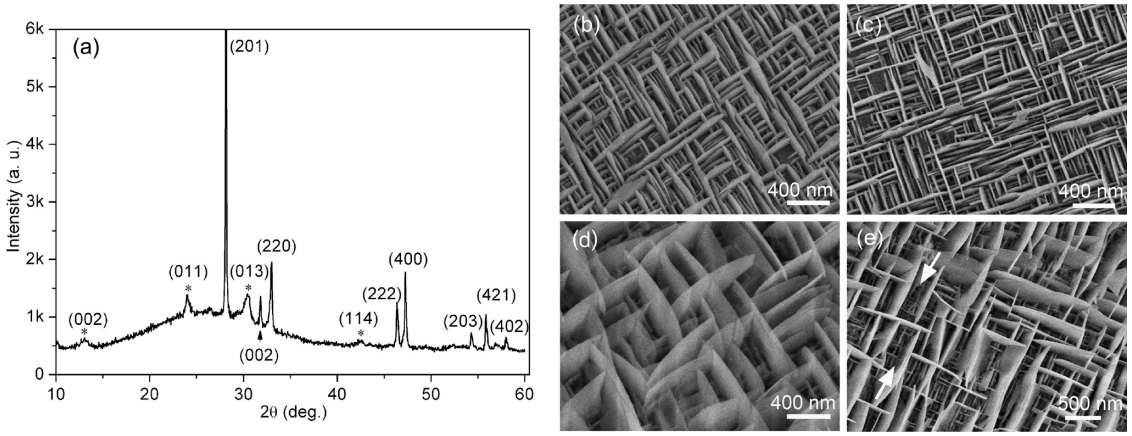

Figure 4. (a) XRD spectrum of $Bi_2O_2CO_3$ 2DONWs heated at 300 °C for 24 h. Besides β-Bi_2O_3, there are several weak peaks that belong to residual $Bi_2O_2CO_3$ (marked with an asterisk (∗)), which will vanish by heating the sample for more than 2 days. (b) Tilt view of a $Bi_2O_2CO_3$ 2DONW. (c) Top view of a β-Bi_2O_3 2DONW transformed from $Bi_2O_2CO_3$ 2DONW. (d) Tilt view of a BiOCl 2DONW from β-Bi_2O_3 2DONW, compared with panel b, the BiOCl nanowalls become much larger. (e) Top view of the BiOCl 2DONW, showing secondary networks indicated by the arrows.

match: the β-Bi_2O_3 has a tetragonal structure with d_{220} = 2.737 Å and it d_{002} = 2.817 Å, both are close to the {110} *d*-spacing (2.734 Å) of $Bi_2O_2CO_3$.

Transformation from $Bi_2O_2CO_3$ 2DONWs to β-Bi_2O_3 and BiOCl 2DONWs and to Bi_2S_3 N2DONWs. $Bi_2O_2CO_3$, as an oxycarbonate, is unstable and it converts to β-Bi_2O_3 by annealing in a temperature range of 260−400 °C, according to

$$Bi_2O_2CO_3 \xrightarrow{\Delta} Bi_2O_3 + CO_2 \qquad (2)$$

We experimentally find that β-Bi_2O_3 can well take the morphology of $Bi_2O_2CO_3$, namely a $Bi_2O_2CO_3$ 2DONW transforms to a β-Bi_2O_3 2DONW. Accordingly, the film turns from white to yellow. The lattice misfit between the {110} facets of $Bi_2O_2CO_3$ and {220} facets of β-Bi_2O_3 is only 0.1%, that means the two phases can almost perfectly match, suggesting a possible epitaxial relationship of $(110)_{Bi_2O_2CO_3}||(220)_\beta$, $(1\bar{1}0)_{Bi_2O_2CO_3}||(2\bar{2}0)_\beta$, and $[001]_{Bi_2O_2CO_3}||[001]_\beta$. The conversion has been proved by X-ray diffraction (XRD) measurement shown in Figure 4a.

The as-formed β-Bi_2O_3 2DONWs convert directly to BiOCl 2DONWs in diluted HCl solution. The formed BiOCl 2DONWs, however, do not take exactly the same morphology of β-Bi_2O_3 2DONWs, but undergo a process in which some nanowalls grow significantly larger. Figure 4 panels b−d show the morphology difference of a $Bi_2O_2CO_3$ 2DONW, corresponding β-Bi_2O_3 2DONW and BiOCl 2DONW. We can see that the β-Bi_2O_3 2DONW is almost the same as the $Bi_2O_2CO_3$ 2DONW, but the BiOCl 2DONW clearly consists of much larger nanowalls, as a result of subsequent growth of BiOCl from the β-Bi_2O_3 nanowalls. Figure 4e shows that in the BiOCl 2DONW there are some secondary networks with smaller features close to that of the β-Bi_2O_3 precursor. For a β-Bi_2O_3 2DONW rinsed in HCl aqueous solution, the surface layer of Bi_2O_3 nanowalls first get dissolved in the acidic solution, releasing BiO^+ (aq) ions; and then the BiO^+ ions combine with Cl^-, forming epitaxial BiOCl on the nondissolved nanowall surface. The most likely case is the small nanowalls get dissolved and large nanowalls grow even larger, and that is why we have large BiOCl nanowalls. It is worth noting that in this conversion the intermediate does not necessarily need to be pure β-Bi_2O_3. $Bi_2O_2CO_3$ 2DONWs partially converted to β-Bi_2O_3 can also lead to a similar morphology of the subsequent BiOCl 2DONWs.

Figure 5a is a bright field TEM image of β-Bi_2O_3 nanowalls, and Figure 5b is a corresponding HRTEM image, showing fringes with a 4-fold symmetry and a spacing of 2.75 Å. The inset taken from the side of a nanowall reveals fringes with a *d*-spacing of 1.12 nm, right twice that of the (001) plane (we could also see the (001) fringes). For Bi_2O_3 nanostructures, such superlattices are common and have been reported in the literature.[20] Figure 5 panels c and d are bright field TEM images of BiOCl nanowalls from $Bi_2O_2CO_3$ and Bi_2O_3, respectively. In good consistence with SEM images, the latter reveals a semicircular shape for nearly 1 μm in length, much larger than its counterpart in panel c. Figure 5 panels e and f are the SAED pattern and HRTEM image of the large BiOCl nanowall. The structural analysis indicates that all nanowalls shown here are single crystalline.

As has been reported, BiOCl 2DONWs transform to Bi_2S_3 N2DONWs by incubating in a blended solution of HCl and TAA in a 60 °C water bath. Both $Bi_2O_2CO_3$ and β-Bi_2O_3 2DONWs can convert to BiOCl nanowalls in diluted HCl solution, and be used as the template for Bi_2S_3 N2DONWs. Here we show Bi_2S_3 N2DONWs converted from β-Bi_2O_3 2DONWs in blended solution of HCl and TAA at 60 °C, as displayed in Figure 6a,b. Additionally Figure 6c is a bright-field TEM image of a Bi_2S_3 network made of two sets of perpendicularly aligned Bi_2S_3 nanorods. The corresponding SAED

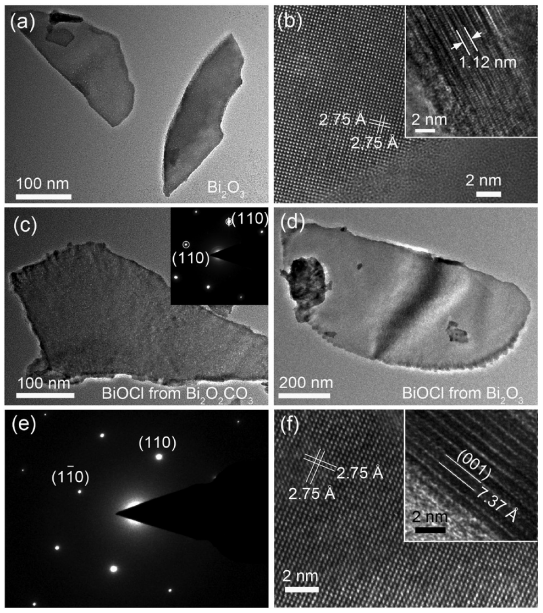

Figure 5. (a) Bright-filed TEM image of β-Bi_2O_3 nanowalls transformed from $Bi_2O_2CO_3$. (b) HRTEM image of a β-Bi_2O_3 nanowall along the [001] zone axis; inset shows side view of a β-Bi_2O_3 nanowall, in which the 1.12 nm fringes belongs to the 1/2(001). (c) TEM image of a BiOCl nanowall transformed from $Bi_2O_2CO_3$; inset is the SAED pattern. (d) TEM image of a BiOCl nanowall transformed from β-Bi_2O_3. (e and f) SAED pattern and HRTEM image of the nanowall in panel d; inset in panel f reveals fringes with a *d*-spacing of 7.37 Å, consistent with the (001) facet of BiOCl.

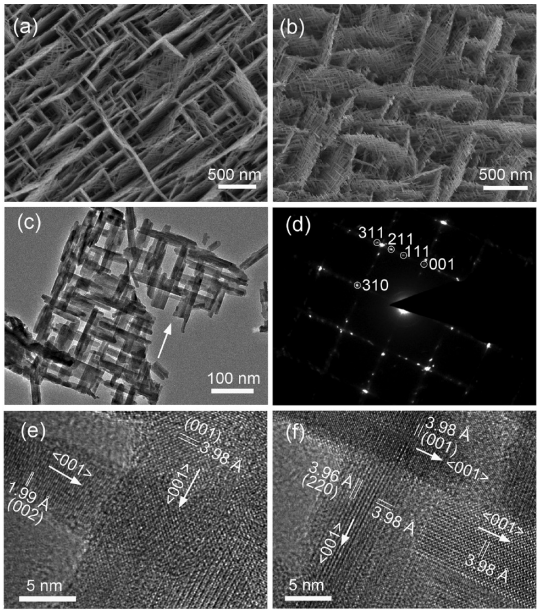

Figure 6. (a) Top view of a Bi_2S_3 N2DONW transformed from β-Bi_2O_3 2DONW. (b) Tilt view of the Bi_2S_3 N2DONW. (c) Bright field TEM image of a Bi_2S_3 network. (d) Corresponding SAED pattern, in which the indexed reflections belong to a set of paralleled Bi_2S_3 nanorods along the direction indicated by the arrow in panel c. (e and f) HRTEM images of woven Bi_2S_3 nanorods, showing all nanorods are along the ⟨001⟩-directions.

pattern (Figure 6d) consists of reflections that belong to two sets of woven nanorods, in accordance with the HRTEM images in Figure 6 panels e and f, in which all the nanorods are along the ⟨001⟩-directions. Our observation upon tens of Bi_2S_3 nanorods indicates that all nanorods are grown along the *c*-axis without exception. However, these nanorods are in fact in different crystal orientations, proven by the reflections of (111), (211), (311) from one set of paralleled ⟨001⟩-oriented nanorods (Figure 6d). The Bi_2S_3 N2DONWs also imply that all nanowall structures in this route, including that of $Bi_2O_2CO_3$, β-Bi_2O_3, and BiOCl, are single crystalline.

BiOCl is a very important intermediate for the formation of superstructured Bi_2S_3 N2DONWs. The $Bi_2O_2CO_3$ or β-Bi_2O_3 2DONWs cannot transform to well ordered Bi_2S_3 N2DONWs with the absence of Cl^-. The products obtained by using a blended solution of TAA and HNO_3 instead of HCl are much different. Supporting Informatioin, Figure S1a is the product transformed from a $Bi_2O_2CO_3$ 2DONW in TAA (0.04 M) and HNO_3 (0.02 M) at 60 °C, showing that the ordering of the Bi_2S_3 networks is much worse than that are formed in blended solution of TAA (0.04 M) and HCl (0.02 M), as shown in Figure S1b. Typically, it takes the $Bi_2O_2CO_3$ film half an hour to turn black (as a sign of the formation of Bi_2S_3) and more than one day to accomplish the transformation. In comparison, in the same environment (0.04 M TAA and 0.02 M HNO_3), the β-Bi_2O_3 2DONWs turn black in tens of seconds, and the product does not present a self-similar structure, but instead each nanowall demonstrates a smooth surface (Figure S1c). It is interesting that the Bi_2S_3 morphology is very sensitive to the concentration of TAA. When the concentration of TAA decreases to 0.02 M, each Bi_2S_3 nanowall becomes rough and consists of many nanoparticles or random nanocones, as shown in Figure S1d. We will show in a further study that β-Bi_2O_3 can transform to Bi_2S_3 nanocones arrays at a low concentration (0.01−0.02 M) of TAA. Unlike β-Bi_2O_3 or $Bi_2O_2CO_3$ 2DONWs, BiOCl 2DONWs could convert directly to self-similar N2DONWs in a blended solution of TAA and HNO_3, or TAA and H_2SO_4 (or TAA and other acids without Cl^-).

The fact that $Bi_2O_2CO_3$ and β-Bi_2O_3 2DONWs could not transform to well ordered Bi_2S_3 N2DONWs should be related to the large lattice misfits with Bi_2S_3 (f = 3.0% and 2.9%, see Table 1). However, an intermediate enables this transformation if it has a smaller lattice misfit with Bi_2S_3, exemplified by the transformation from β-Bi_2O_3 to BiOCl and finally to Bi_2S_3 N2DONWs. The reaction from β-Bi_2O_3 directly to Bi_2S_3 is too fast might be another reason that we did not see any ordered Bi_2S_3 nanorods formed on the β-Bi_2O_3 nanowalls.

Thermal Oxidation of Bi_2S_3 N2DONWs. Thermal oxidation of Bi_2S_3 N2DONWs has also been investigated as we expected to obtain β-Bi_2O_3 N2DONWs. A Bi_2S_3 N2DONWs heated at 320 °C for 3 h is found to convert

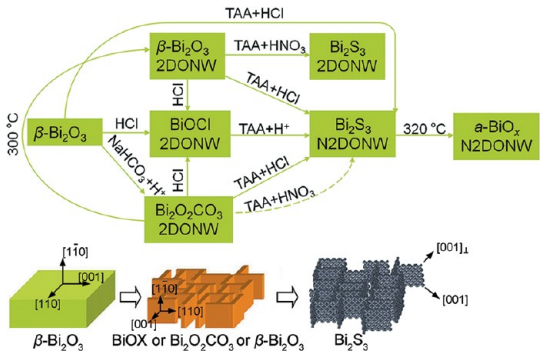

Figure 7. Routes from β-Bi_2O_3 to various superstructured bismuth compounds.

to amorphous BiO_x N2DONWs instead of β-Bi_2O_3 structures. Accordingly, the black sample turns to semitransparent. Supporting Information, Figure S2a is a SEM image of an amorphous BiO_x N2DONW, while Figure S2 panels b and c are corresponding TEM image and HRTEM image. The corresponding SAED pattern of such a network, however, reveals a 4-fold symmetry, and weak reflections correspond to an interplanar spacing of ~2.75 Å, which seems to be consistent with the {220} facets of β-Bi_2O_3. This is in contradiction with the fact that although the precursor Bi_2S_3 nanorods grow along the ⟨001⟩-directions, they are actually not in the same crystal orientations. A possible explanation is that the weak reflections belong to residual BiOCl, which is right 4-fold symmetric in the [001]-direction with the interplanar spacing of {110} to be 2.75 Å. As we know, it takes at least two days for a BiOCl nanowall to convert to Bi_2S_3 network completely, but we typically spend only one day for the conversion, so that it is reasonable to have residual BiOCl in the networks.

Another sample annealed for 32 h is quite different, for which the networks have been completely destroyed and transformed to nanoparticles, as shown in Figure S2d. During the long time annealing, the amorphous nanorods (which are formed in the first several hours of heating) cannot convert to single crystalline nanorods again, instead, many Bi_2O_3 nanoparticles are formed in the long heating time.

Corrosion, Epitaxial Nucleation, and Growth. The networks of bismuth compounds are epitaxially formed from the single crystalline β-Bi_2O_3. How new crystalline phases emerge is rather important and interesting. Here we discuss the nucleation and growth of the bismuth compounds.

Take the formation of BiOCl for example. A single crystalline β-Bi_2O_3 domain in diluted hydrochloric acid is first etched by H^+ (aq), and the released BiO^+ ions incorporate with Cl^- (aq) in the liquid−solid interface, leading to the formation of epitaxial BiOCl nuclei. The BiOCl nuclei form in the liquid−solid interface rather than in the solution, because heterogeneous nucleation and epitaxial growth can efficiently decrease the surface energy of the system. The epitaxial BiOCl nuclei grow up to nanowalls because the weak nonbonding interaction between *c*-planes can result in strongly anisotropic growth. And the lattice-directing guides orientation of the nanowalls, which finally construct an orthogonal network. The formation of $Bi_2O_2CO_3$ networks is in a very similar process.

For the formation of the Bi_2S_3 network, the template, BiOCl nanowall is first etched by H^+ (aq). Then epitaxial Bi_2S_3 nuclei are formed in the surface of BiOCl, and the nuclei grow up and form rodlike structures. The reaction can be expressed as

$$2BiOCl + 3S^{2-} + 4H^+ \rightarrow 2Bi_2S_3\downarrow + 2H_2O + 2Cl^- \quad (3)$$

Because BiOCl is indissoluble, it takes a long time to complete the reaction. An acidic environment is also very necessary for this process. We have observed that networks of Bi_2S_3 cannot be formed with the absence of acid, and the concentration of H^+ influences significantly the size and morphology of Bi_2S_3 nanostructures. Generally speaking, a higher concentration of H^+ will cause coarsening of nanorods.

The crystalline superstructures fabricated in this study are all formed upon the epitaxial relationships among the phases. Here we summarize these transformations in Figure 7, which shows that a β-Bi_2O_3 crystal domain could convert to a BiOX (X = Cl or Br, and we only show BiOCl here), or $Bi_2O_2CO_3$ 2DONW; the $Bi_2O_2CO_3$ 2DONW converts to BiOCl 2DONW in diluted HCl, or to β-Bi_2O_3 2DONW by annealing at ~300 °C for tens of hours; the β-Bi_2O_3, BiOX, or $Bi_2O_2CO_3$ 2DONW can act as an intermediate template for the formation of Bi_2S_3 N2DONW in a preblended solution of TAA and HCl at 60 °C. All the tetragonal phases, including BiOX (X = Cl or Br), β-Bi_2O_3, and $Bi_2O_2CO_3$, have a lattice parameter $a \approx 2^{n/2} \times 3.9$ Å ($n = 0$ or 2), and this matches the lattice parameter *c* of the orthorhombic Bi_2S_3. We believe that there will be much more bismuth compounds that can present the unique morphology of 2DONW or N2DONW in a lattice directed process.

CONCLUSION

We have successfully demonstrated the fabrication of superstructured 2DONWs of BiOX (X = Cl, Br), $Bi_2O_2CO_3$, β-Bi_2O_3, and Bi_2S_3, as well as self-similar N2DONWs of Bi_2S_3, in a series of lattice-directed transformations. The β-Bi_2O_3 single crystalline domains serve as the precursor of the superstructures. All phases involved in this work have a lattice parameter of $\sim 2^{n/2} \times 3.9$ Å ($n = 0, 1, 2, 3, 4$). We predict that many other bismuth compounds with a 4-fold symmetry of quasi 4-fold symmetry and a lattice parameter close to $\sim 2^{n/2} \times 3.9$ Å ($n = 0, 1, 2, 3, 4$), for example, γ-Bi_2O_3, δ-Bi_2O_3, $Bi_2O_{2.33}$, $BiFeO_3$, Bi_2O_2Se, $C_2H_3BiO_3$, Bi_2WO_6, Bi_2MoO_6, and Bi_2VO_5, may also present the unique morphologies of 2DONW or N2DONW. Also the use of single crystalline substrates with lattice match may enable the formation of a 2DONW or N2DONW on

wafer scale. The superstructures are expected to find applications that require gridlike structure or large specific surface. Additionally, the Bi_2S_3 networks have been found to have excellent resistance switching property and good thermoelectric property, which will be discussed in our further works.

EXPERIMENTAL SECTION

Amorphous BiO_x films by reactive magnetron sputtering were heated at 300−500 °C to produce β-Bi_2O_3 films. For the transformation from β-Bi_2O_3 to Bi_2S_3 N2DONWs, a β-Bi_2O_3 film was incubated in blended solution of TAA (0.04 M) and HCl (0.02 M) for 1−3 days, or blended solution of TAA (0.04 M), NaBr (0.02 M), and H_2SO_4 (0.01 M) at a water bath temperature of 60 °C. $Bi_2O_2CO_3$ 2DONWs were formed with a β-Bi_2O_3 film incubating in a blended solution of $NaHCO_3$ (0.04 M) and HNO_3 (0.02 M) at 60 °C for 5 h. β-Bi_2O_3 2DONWs were formed by thermal annealing of the $Bi_2O_2CO_3$ 2DONWs at 320 °C for 1−3 days. The as-formed β-Bi_2O_3 2DONWs transformed to BiOCl 2DONWs in diluted HCl solution (0.1 M) for minutes, or transformed to Bi_2S_3 N2DONWs in blended solution of TAA (0.04 M) and HCl (0.02 M) for tens of hours. Two Bi_2S_3 N2DONW samples were annealed at 320 °C for 3 and 32 h, respectively, forming amorphous BiO_x N2DONWs.

The morphology of the samples was observed by SEM (Hitachi S-4800) and TEM (FEI Tecnai G^2 F20). Crystal structure analysis was made by using HRTEM, SAED (with the FEI Tecnai G^2 F20 microscope), and XRD (Bruker D8 Focus).

Conflict of Interest: The authors declare no competing financial interest.

Acknowledgment. This work was supported by the funds from NSFC (10974037), NBRPC (2010CB934102), International S&T Cooperation Program (2010DFA51970), and Eu-FP7 (No. 247644).

Supporting Information Available: Two electron micrographs on the transformation from $Bi_2O_2CO_3$ 2DONWs to Bi_2S_3 nanostructure with different conditions and the transformation from Bi_2S_3 N2DONWs to amorphous BiO_x N2DONWs. This material is available free of charge *via* the Internet at http://pubs.acs.org.

REFERENCES AND NOTES

1. Huang, M. H.; Wu, Y.; Feick, H.; Tran, N.; Weber, E.; Yang, P. Catalytic Growth of Zinc Oxide Nanowires by Vapor Transport. *Adv. Mater.* **2011**, *3*, 113–116.
2. Duan, X.; Huang, Y.; Cui, Y.; Wang, J.; Lieber, C. M. Indium Phosphide Nanowires as Building Blocks for Nanoscale Electronic and Optoelectronic Devices. *Nature* **2001**, *409*, 66–69.
3. Xia, Y.; Yang, P.; Sun, Y.; Wu, Y.; Mayers, B.; Gates, B.; Yin, Y.; Kim, F.; Yan, H. One-Dimensional Nanostructures: Synthesis, Characterization and Applications. *Adv. Mater.* **2003**, *15*, 353–389.
4. He, J. H.; Yang, R. S.; Chueh, Y. L.; Chou, L. J.; Chen, L. J.; Wang, Z. L. Aligned AlN Nanorods with Multi-tipped Surfaces—Growth, Field-Emission, and Cathodoluminescence Properties. *Adv. Mater.* **2006**, *18*, 650–654.
5. Xu, S.; Wei, Y.; Fang, H.; Kirkham, M.; Liu, J.; Mai, W.; Davidovic, D.; Snyder, R. L.; Wang, Z. L. Patterned Growth of Vertically Aligned ZnO Nanowire Arrays on Inorganic Substrates at Low Temperature without Catalyst. *J. Am. Chem. Soc.* **2008**, *130*, 14958–14959.
6. Pan, Z. W.; Dai, Z. R.; Wang, Z. L. Nanobelts of Semiconducting Oxides. *Science* **2001**, *291*, 1947–1949.
7. Sun, Y.; Mayers, B.; Xia, Y. Transformation of Silver Nanospheres into Nanobelts and Triangular Nanoplates through a Thermal Process. *Nano Lett.* **2003**, *3*, 675–679.
8. Kong, X. Y.; Ding, Y.; Yang, Ru.; Wang, Z. L. Single-Crystal Nanorings Formed by Epitaxial Self-Coiling of Polar Nanobelts. *Science* **2004**, *303*, 1348–1351.
9. Lao, J. Y.; Wen, J. G.; Ren, Z. F. Hierarchical ZnO Nanostructures. *Nano Lett.* **2002**, *2*, 1287–1291.
10. Guo, C. F.; Wang, Y.; Jiang, P.; Cao, S.; Miao, J.; Zhang, Z.; Liu, Q. Zinc Oxide Nanostructures: Epitaxially Growing from Hexagonal Zinc Nanostructures. *Nanotechnology* **2008**, *19*, 445710.
11. Wan, Q.; Wei, M.; Zhi, D.; MacManus-Driscoll, J. L.; Blamire, M. G. Epitaxial Growth of Vertically Aligned and Branched Single-Crystalline Tin-Doped Indium Oxide Nanowire Arrays. *Adv. Mater.* **2006**, *18*, 234–238.
12. Cheng, C. W.; Liu, B.; Yang, H. Y.; Zhou, W. W.; Sun, L.; Chen, R.; Yu, S. F.; Gong, H.; Zhang, J. X. H.; *et al.* Hierarchical Assembly of ZnO Nanostructures on SnO_2 Backbone Nanowires: Low Temperature Hydrothermal Preparation and Optical Properties. *ACS Nano* **2009**, *3*, 3069–3076.
13. Liu, J. P.; Jiang, J.; Cheng, C. W.; Li, H. X.; Zhang, J. X.; Gong, H.; Fan, H. J. Co_3O_4 Nanowire@MnO_2 Ultrathin Nanosheet Core−Shell Arrays: A New Class of High-Performance Pseudocapacitive Materials. *Adv. Mater.* **2011**, *23*, 2076–2081.
14. Gao, M.-R.; Liu, S.; Jiang, J.; Cui, C.-H.; Yao, W.-T.; Yu, S.-H. *In Situ* Controllable Synthesis of Magnetite Nanocrystals/$CoSe_2$ Hybridnanobelts and Their Enhanced Catalytic Performance. *J. Mater. Chem.* **2010**, *20*, 9355–9361.
15. Guo, C. F.; Cao, S.; Zhang, J.; Tang, H.; Guo, S.; Tian, Y.; Liu, Q. Topotactic Transformations of Superstructures: From Thin Films to 2D Networks to Nested 2D Networks. *J. Am. Chem. Soc.* **2011**, *133*, 8211–8215.
16. Peng, H.; Chan, C. K.; Meister, S.; Zhang, X. F.; Cui, Y. Shape Evolution of Layer-Structured Bismuth Oxychloride Nanostructures *via* Low-Temperature Chemical Vapor Transport. *Chem. Mater.* **2009**, *21*, 247–252.
17. Cao, S.; Guo, C.; Lv, Y.; Guo, Y.; Liu, Q. A Novel BiOCl Film with Flower-like Hierarchical Structure and Its Optical Properties. *Nanotechnology* **2009**, *20*, 275702.
18. Bannister, F. A.; Hey, M. H. The Crystal Structure of The Bismuth Oxyhalides. *Mineral. Mag.* **1935**, *149*, 49–58.
19. Li, L.; Sun, N.; Huang, Y.; Qin, Y.; Zhao, N.; Gao, J.; Li, M.; Zhou, H.; Qi, L. Topotactic Transformation of Single-Crystalline Precursor Discs into Disc-Like Bi_2S_3 Nanorod Networks. *Adv. Funct. Mater.* **2008**, *18*, 1194–1201.
20. Zhou, W.; Jefferson, D. A.; Alario-Franco, M.; Thomas, J. M. Superlattices in Ternary Oxides Derived from Bismuth Oxide (Bi_2O_3): New Families of Ordered Phases Based on The Fluorite Structure. *J. Phys. Chem.* **1987**, *91*, 512–514.